AFRL-RQ-WP-TR-2014-0050

SPATIALLY TARGETED ACTIVATION OF A SHAPE MEMORY, POLYMER-BASED, RECONFIGURABLE SKIN SYSTEM

James J. Joo and Gregory W. Reich

Design and Analysis Branch
Aerospace Vehicles Division

Richard V. Beblo

University of Dayton Research Institute

FEBRUARY 2014
Final Report

AIR FORCE RESEARCH LABORATORY
AEROSPACE SYSTEMS DIRECTORATE
WRIGHT-PATTERSON AIR FORCE BASE, OH 45433-7542
AIR FORCE MATERIEL COMMAND
UNITED STATES AIR FORCE

NOTICE AND SIGNATURE PAGE

Using Government drawings, specifications, or other data included in this document for any purpose other than Government procurement does not in any way obligate the U.S. Government. The fact that the Government formulated or supplied the drawings, specifications, or other data does not license the holder or any other person or corporation; or convey any rights or permission to manufacture, use, or sell any patented invention that may relate to them.

This report was cleared for public release by the USAF 88th Air Base Wing (88 ABW) Public Affairs Office (PAO) and is available to the general public, including foreign nationals.

Copies may be obtained from the Defense Technical Information Center (DTIC) (http://www.dtic.mil).

AFRL-RQ-WP-TR-2014-0050 HAS BEEN REVIEWED AND IS APPROVED FOR PUBLICATION IN ACCORDANCE WITH ASSIGNED DISTRIBUTION STATEMENT.

*//Signature//

JAMES J. JOO, Engineer
Design and Analysis Branch
Aerospace Vehicles Division

//Signature//

THOMAS C. CO, Branch Chief
Design and Analysis Branch
Aerospace Vehicles Division

//Signature//

FRANK WITZEMAN, Chief
Aerospace Vehicles Division
Aerospace Systems Directorate

This report is published in the interest of scientific and technical information exchange, and its publication does not constitute the Government's approval or disapproval of its ideas or findings.

*Disseminated copies will show "//Signature//" stamped or typed above the signature blocks.

REPORT DOCUMENTATION PAGE

Form Approved
OMB No. 0704-0188

1. REPORT DATE *(DD-MM-YY)*	2. REPORT TYPE	3. DATES COVERED *(From - To)*
February 2014	Final	01 October 2011 – 30 September 2013

4. TITLE AND SUBTITLE
SPATIALLY TARGETED ACTIVATION OF A SHAPE MEMORY, POLYMER-BASED, RECONFIGURABLE SKIN SYSTEM

5a. CONTRACT NUMBER
In-house

5b. GRANT NUMBER

5c. PROGRAM ELEMENT NUMBER
62201F

6. AUTHOR(S)
James J. Joo and Gregory W. Reich (AFRL/RQVC)
Richard V. Beblo (University of Dayton Research Institute)

5d. PROJECT NUMBER
2401

5e. TASK NUMBER
N/A

5f. WORK UNIT NUMBER
Q0Q0

7. PERFORMING ORGANIZATION NAME(S) AND ADDRESS(ES)
Design and Analysis Branch (AFRL/RQVC)
Aerospace Vehicles Division
Air Force Research Laboratory, Aerospace Systems Directorate
Wright-Patterson Air Force Base, OH 45433-7542
Air Force Materiel Command, United States Air Force

University of Dayton
Research Institute
300 College Park
Dayton, OH 45469

8. PERFORMING ORGANIZATION REPORT NUMBER
AFRL-RQ-WP-TR-2014-0050

9. SPONSORING/MONITORING AGENCY NAME(S) AND ADDRESS(ES)
Air Force Research Laboratory
Aerospace Systems Directorate
Wright-Patterson Air Force Base, OH 45433-7542
Air Force Materiel Command
United States Air Force

10. SPONSORING/MONITORING AGENCY ACRONYM(S)
AFRL/RQVC

11. SPONSORING/MONITORING AGENCY REPORT NUMBER(S)
AFRL-RQ-WP-TR-2014-0050

12. DISTRIBUTION/AVAILABILITY STATEMENT
Approved for public release; distribution unlimited.

13. SUPPLEMENTARY NOTES
PA Case Number: 88ABW-2014-0630; Clearance Date: 20 Feb 2014. This report contains color.

14. ABSTRACT
The objective of the project is to investigate the thermo-mechanical behavior of engineered shape memory polymer (SMP) materials for use as composite reconfigurable skin systems in morphing aircraft applications. An anisotropic, reconfigurable skin based on selective heating of a cellular SMP material was designed and investigated to understand its material characteristics. The engineered skin material is made of a cellular structure filled with a variable stiffness material, such as honeycomb filled with SMP and it was characterized by finite element analysis and MTS testing. The research provides a comprehensive initial feasibility study into the proposed filled honeycomb skin system, and thermal problems such as diffusion between cells, cooling the skin, the power required for operation, and cycle time are topics of further research.

15. SUBJECT TERMS
reconfigurable skin, shape memory polymer, honeycomb structure

16. SECURITY CLASSIFICATION OF:			17. LIMITATION OF ABSTRACT:	18. NUMBER OF PAGES	19a. NAME OF RESPONSIBLE PERSON (Monitor)
a. REPORT	b. ABSTRACT	c. THIS PAGE			James J. Joo
Unclassified	Unclassified	Unclassified	SAR	42	19b. TELEPHONE NUMBER *(Include Area Code)* (937) 713-7137

TABLE OF CONTENTS

LIST OF FIGURES

Figure **Page**

LIST OF TABLES

Table **Page**

PREFACE

Reconfigurable structures have been the topic of much research in recent years including candidate materials and systems used to cover them, skins. It has also been proposed that the skin covering the wing of a reconfigurable aircraft could be made of a cellular structure filled with a variable stiffness material, such as honeycomb filled with shape memory polymer (SMP). The presented work outlines an initial investigative effort to determine the feasibility of such a system, mechanically characterize the system given chosen candidate materials, and develop an optimization scheme for tailoring the system to specific applications. The chosen candidate materials of epoxy shape memory polymer and aluminum honeycomb are individually characterized. Using these materials, the Young's moduli and shear moduli of the filled honeycomb composite are also experimentally determined above and below the transition temperature of the polymer. These results are then used to validate an analytical model taking into account the geometry of the honeycomb. A finite element analysis is also presented for comparison with the experimental results and analytic model. Once validated, the analytic model is then used in an optimization scheme to optimize the honeycomb geometry given an assumed set of constraints and desired skin properties. Finally, limitations of each element of the analysis and future work are discussed.

1.0 INTRODUCTION

The aerodynamic performance of aircraft for specific mission profile segments can be improved through changes in wing shape (Andersen, 2007). Andersen showed that in a variety of mission segments such as dash, cruise, climb, and loiter a different wing configuration optimized aerodynamic performance. The current goal is to create a monolithic skin that does not wrinkle when deformed and is able to strain more than traditional materials while supporting aerodynamic loads.

Cellular structures can be designed with relatively low in-plane and high out-of-plane stiffness. Low stiffness is obtained by the empty space within each cell, providing space for the nearby thin structures to deform. Deformation of these thin beam structures can be inhibited by filling the empty space or by adhering face sheets. Thus the stiffness of the cellular composite can be controlled by judicious choice of materials. If a phase change or variable stiffness material such as shape memory polymer is used, the effective stiffness of the skin is controllable both in magnitude and direction. By heating individual cells, such as shown in Figure 1, in specific patterns the global material properties of the skin can be tailored to the specific in-flight needs of the aircraft. A few potential heating patterns are shown in Figure 2. The following is an experimental investigation into the possible range of effective skin properties, representing bounded limits of the system.

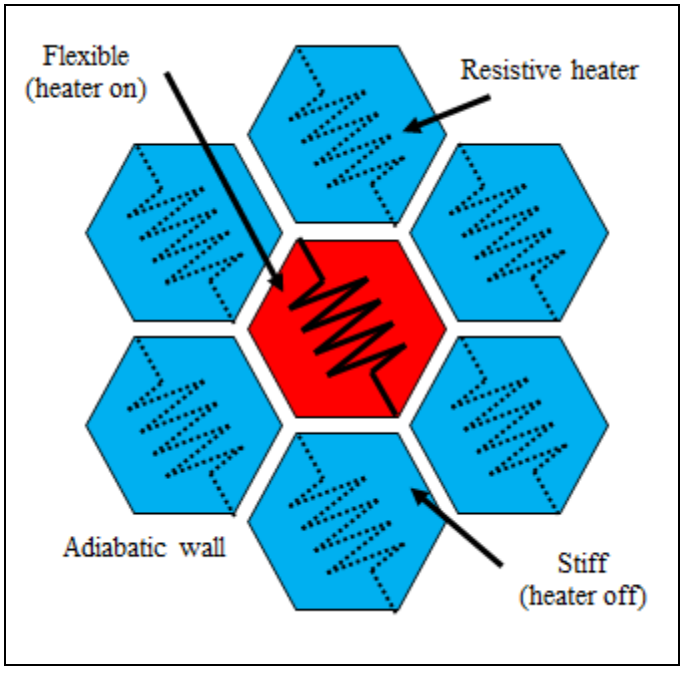

Figure 1: Filled Honeycomb Concept

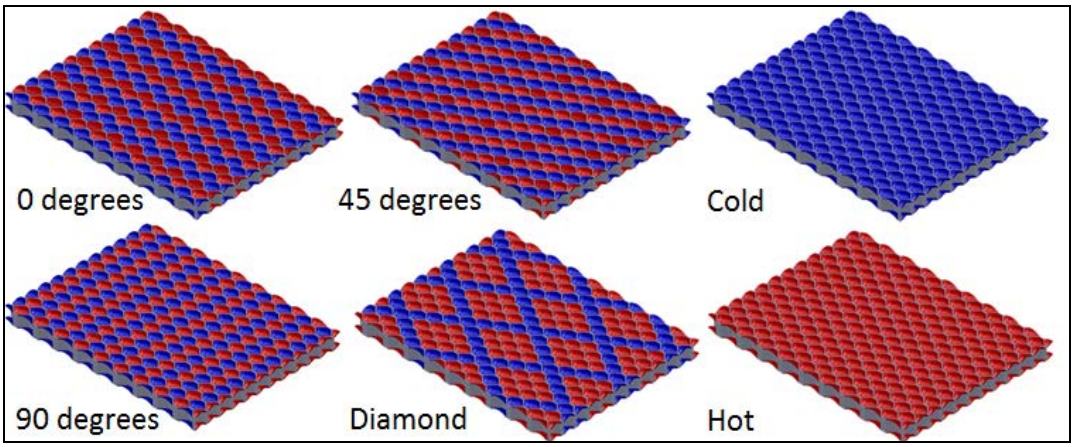

Figure 2: Conceptual Heating Patterns

The goal of the presented research is to experimentally validate, model, and optimize filled honeycomb for use as a reconfigurable skin. This was accomplished by experimentally characterizing the epoxy SMP, aluminum honeycomb, and SMP/honeycomb composite at ambient and above T_g temperatures in both in-plane cardinal directions. This data along with finite element analysis (FEA) was then used to validate an analytical model. Finally, using the experimentally validated analytical model, topology optimization on the composite skin was performed to find the ideal honeycomb geometry given a prescribed set of boundary conditions.

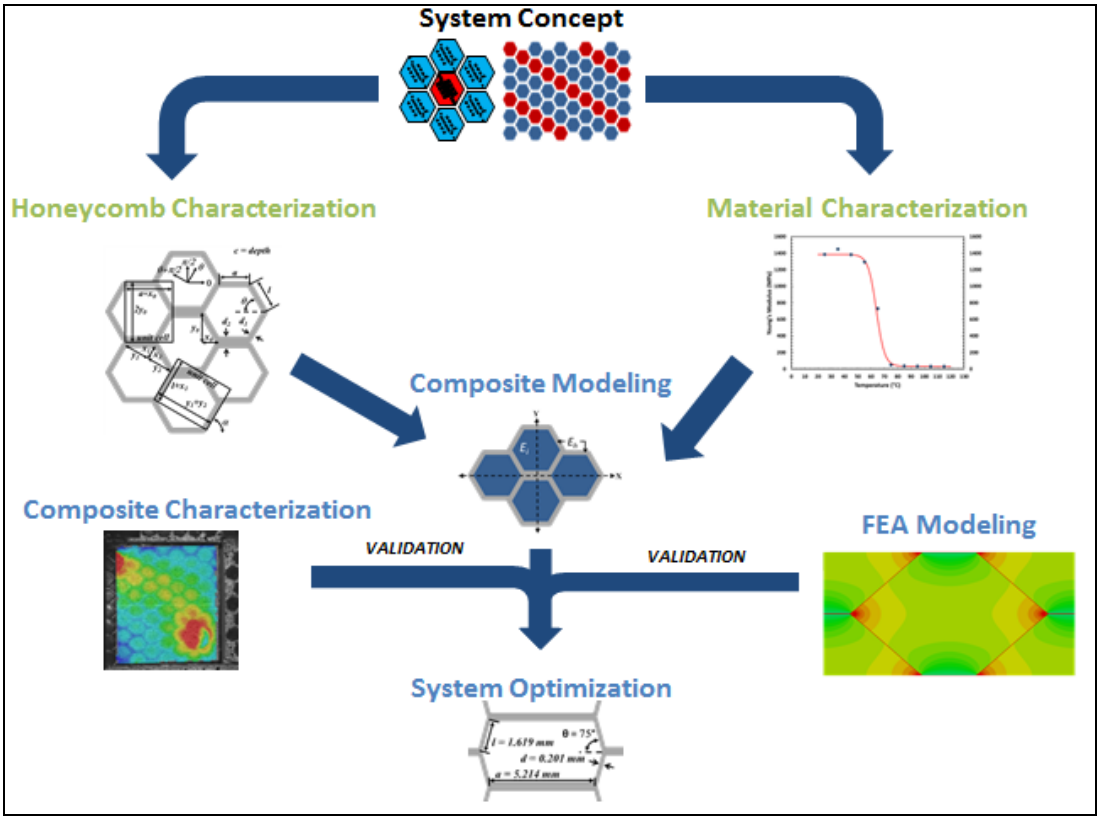

Figure 3: Project Road Map

2.0 NEAT EPOXY SMP CHARACTERIZATION

To eliminate availability issues, in-house epoxy SMP was used. To ensure proper manufacture, repeatability, and for use with the analytical and FEA models; tensile, compressive, and shear moduli above and below T_g were found experimentally as well as the glass transition temperature, T_g.

2.1 Sample Preparation

SMP was chosen as the infill for its ease of manufacturing, light weight, and mechanical properties. Epoxy SMP developed by GM Research and Development consisting of EPON 826 and Jeffamine D230 was mixed and cured in sheets in a Teflon mold according to published guidelines. (Xie and Rousseau, 2009) The resulting sheets were then either tested as is in shear or cut into dog-bone samples described in ASTM Standard D638 using a CNC router. Compression test samples were cured in an aluminum cylinder mold treated with mold release with Teflon end plugs and cut to length with a small lathe.

2.2 Tensile/Compressive Tests

Tensile tests were conducted on a MTS QTest/1L Elite screw driven machine under displacement control with a 50-lb load cell. A B&K Precision 720 K-Type Thermocouple Reader measured the temperature while a custom thermal chamber was manufactured using Fiberfrax©. Heat was supplied by a heat pipe connected to house compressed air. Both tensile and compression tests were conducted at approximately 2 percent strain per minute.

Each sample was tested below the yield stress of the material at several temperatures between ambient and 130 °C. The modulus of the material at each temperature was calculated using linear regression in Matlab®. A modified Heaviside function was then fit to each sample calculating the hard and soft state moduli and the transition temperature, T_g.

$$E(T) = (E_C - E_H)\left[1 - \frac{1}{1 - e^{-2S(T - T_g)}}\right] + E_H \tag{1}$$

Where E is Young's modulus, T is temperature, and the subscripts C and H represent the cold and hot states of the polymer, respectively. T_g and S are dependent variables. Figure 4 shows six representative tensile tests and associated Heaviside functions and error. The error listed in Table 1 represents a 95-percent confidence interval. Numerous samples were tested over a 3-month span with no discernible effects from relative humidity, oxidation, or off-gassing.

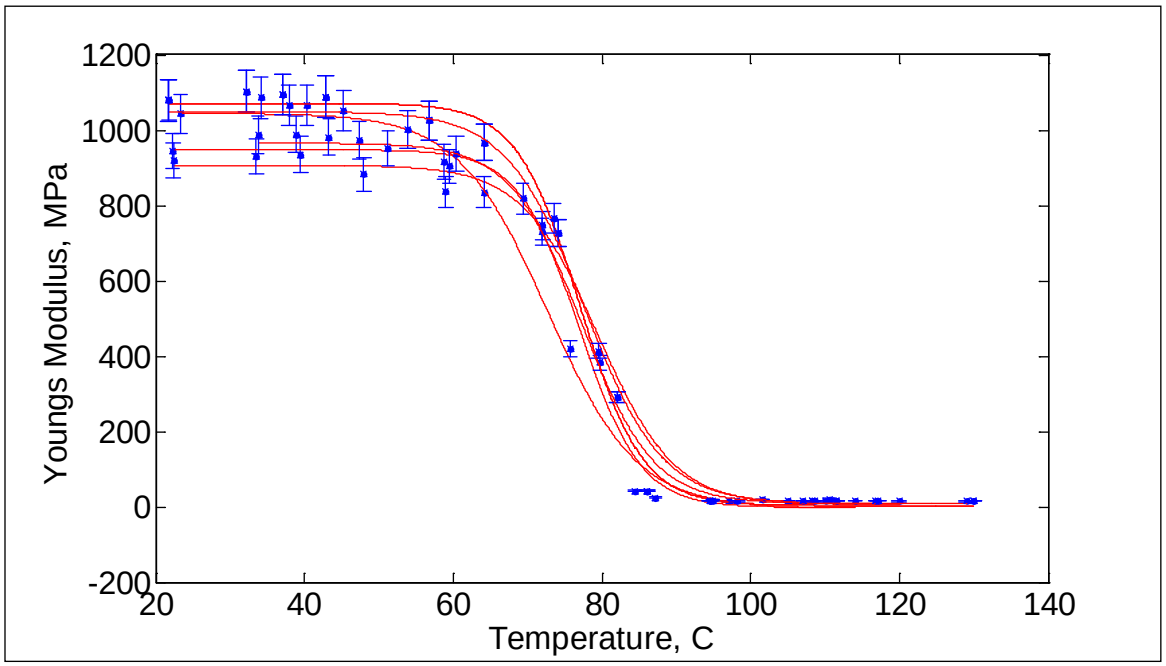

Figure 4: SMP Modulus and Associated Heaviside Functions

Table 1: Neat Epoxy SMP Results

	Young's Modulus (MPa)	
	$< T_g$	$> T_g$
Tension	1300±120	19±3.1
Compression	NA	14±0.7

2.3 Shear Test

The shear modulus of the SMP was also tested using the same custom test fixture, procedure, and sample type described in Section 4.2. Only one sample was tested due to time constraints, which failed along the diagonal. The cold state shear modulus was calculated to be 1.27 GPa while the soft state modulus was found to be 1.06 MPa.

3.0 ALUMINUM HONEYCOMB CHARACTERIZATION

Tensile tests were also conducted on empty honeycomb at various angles for use in a subsequent analytical model. ASTM standard test method C 363/C 363M – 09 for Node Tensile Strength of Honeycomb Core Materials was used. Aluminum 3003 honeycomb was purchased from McMaster Carr with measured dimensions shown in Table 2 and defined in Figure 5.

Table 2: Experimental Honeycomb Properties

a Horizontal Wall Length (mm)	*l* Slanted Wall Length (mm)	*d* Wall Thickness (mm)	*c* Honeycomb Depth (mm)	θ Interior Angle (deg)
5.327	9.28	0.044	6.44	45.964

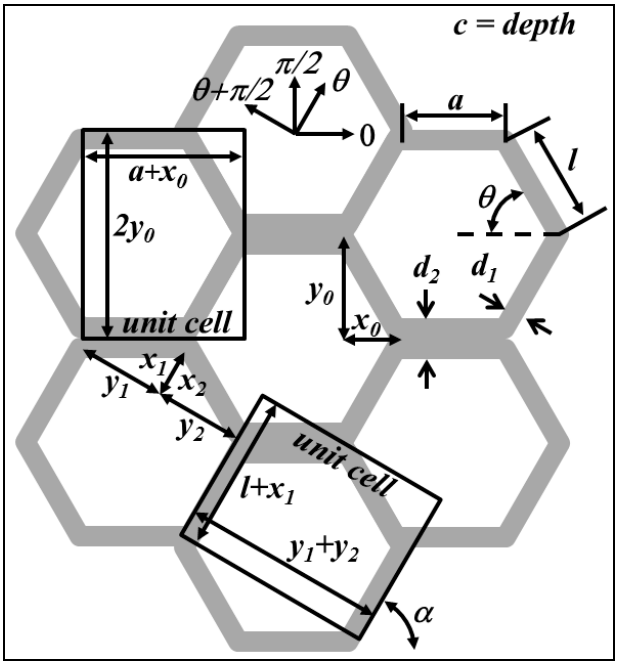

Figure 5: Honeycomb Geometry and Variable Definitions

The honeycomb was cut into 130 x 260 mm segments with scissors using a template to ensure repeatability. Tests were conducted on an MTS ATest/1L Elite screw driven load frame with a 50lb load cell. Custom test grips were made of aluminum and are shown in Figure 6. Tests were conducted at 4 mm/min, approximately 2-percent strain per minute. The error shown in Table 3 represents a 95-percent confidence interval over eight samples.

Figure 6: Empty Honeycomb Tensile Test in the Y Direction

Table 3: Empty Honeycomb Results

Angle (α)	Young's Modulus (Pa)
0°	5.55E4 ± 1.17E4
15°	4.72E5 ± 0.58E5
30°	7.83E5 ± 1.30E5
45°	6.37E5 ± 0.72E5
90°	2.01E4 ± 1.83E4

The effective in-plane stiffness of the honeycomb at arbitrary angles between 0° and 90° was found to be an order of magnitude higher than those at 0° and 90°. This was expected due to the geometry of the tested honeycomb having horizontal members, *a*, much shorter than slanted members, *l*. As can be seen in Figure 7, when the honeycomb is tested at 45°, the force is nearly axial to the slanted members. Since the major mode of deformation is bending, the horizontal members are much shorter than the slanted members, and bending force scales with length cubed, the effective stiffness in this direction is much greater than at 0° or 90°. A similar argument explains the elevated stiffness at 30°, with the force being nearly axial to both the horizontal and slanted honeycomb members. If the length of *a* equals *l* and θ is 60° representing a standard honeycomb, the effective stiffness is nearly isotropic. Anisotropies of

irregular geometries could potentially be utilized in the design of reconfigurable skins where preferential directions of deformation are desired.

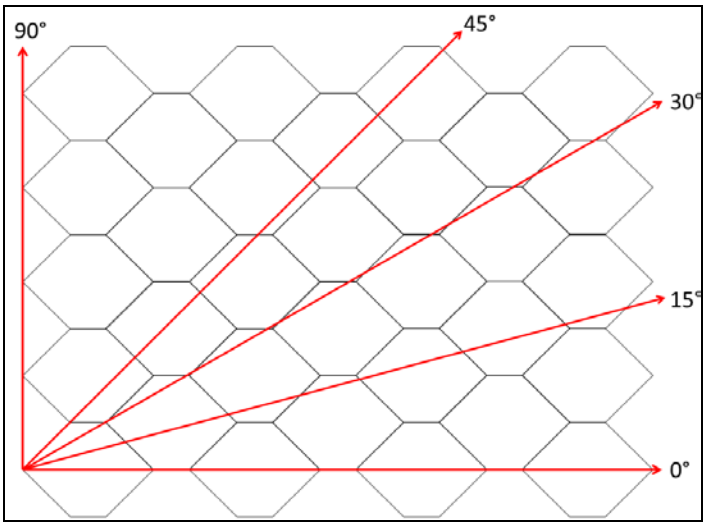

Figure 7: Experimental Honeycomb Geometry with Tested Orientations

4.0 HONEYCOMB/SMP COMPOSITE CHARACTERIZATION

4.1 Composite Tensile Testing

For tensile tests, ¼ inch thick aluminum 3003 honeycomb from McMaster-Carr with dimensions shown in Table 2 was cut into 130 by 260 mm samples using a template similar to those used for empty honeycomb tests. The honeycomb was then soaked in a nitric acid bath at 23.5-percent concentration for 10 minutes, rinsed, and placed in an oven at 100°C for 20 minutes to dry. Etching the honeycomb removed any oil residue from manufacturing and improved adhesion between the aluminum and SMP. Epoxy SMP was then poured into a Teflon mold filling the honeycomb in three stages: 1) providing a thin layer on the bottom to isolate each cell and cured for one hour at 100°C, 2) every other row of cells was filled and cured for an hour at 100°C, and 3) the remaining cells were filled and the sample cured for an additional three hours at 100°C. Weights were placed on top of the honeycomb during curing to keep it flush with the top of the mold. For hard state tensile tests 2.54 cm by 12.7 cm by 0.3175 cm aluminum plates were epoxied to the top and bottom of the sample to help distribute loads during testing and aid in gripping the sample.

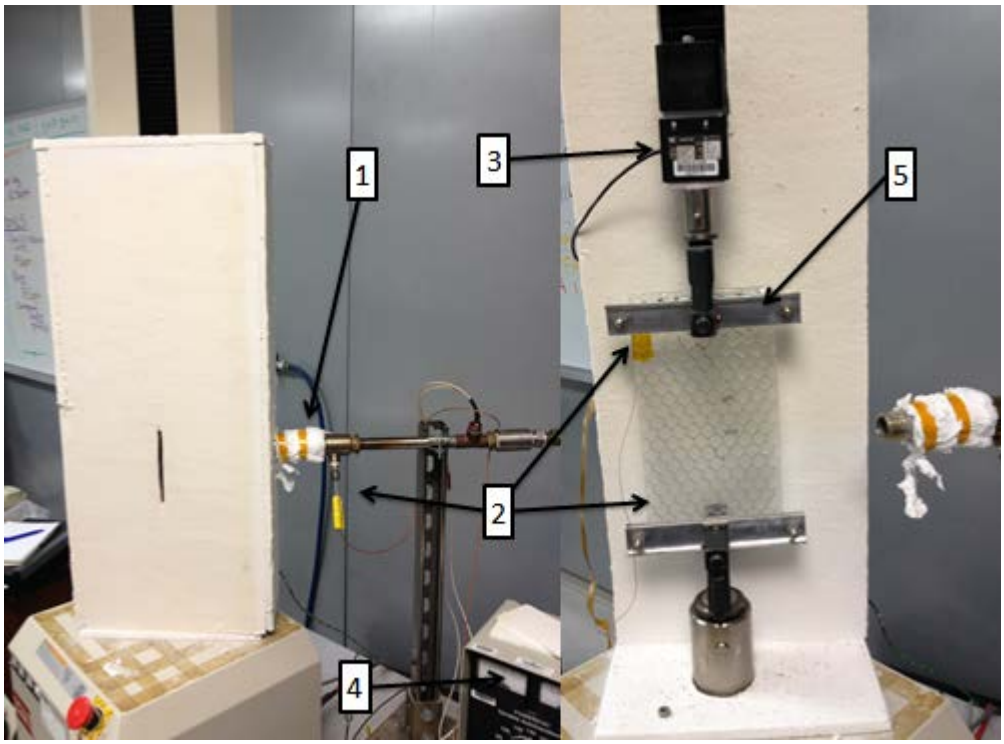

Figure 8: Tensile Test Setup – Left; Enclosed Thermal Chamber Right
1: Heat Pipe 2: Thermocouples 3: 50lb Load Cell 4: Heater Power Source 5: Aluminum Plates Used to Attach the Specimen

A MTS ATest/1L screw driven load frame with a 50lb load cell was used for soft state testing. The thermal chamber was made out of Fiberfrax® and the temperature controlled using a custom heat pipe using house compressed air. A K-type thermocouple and a B&K Precision 720 K-Type Thermocouple Reader were used to measure temperature. Soft state tests were conducted at approximately 110°C.

Hard state tensile tests were conducted on a MTS 20kip hydraulic load frame with a Sintech Model 3187-104 20,000lb load cell. The specimen was attached with 3-inch hydraulically actuated grips. Both hard and soft state tests were conducted at 12.7 mm/min strain rate, approximately 2 percent strain per minute. The errors listed in Table 4 are 95 percent confidence intervals over eight samples.

Table 4: Experimental Results for SMP Filled Honeycomb in Tension

Temperature	Direction	Tensile Modulus (Pa)
$< T_g$	0°	2.19E9 ± 0.08E9
	90°	2.04E9 ± 0.10E9
$> T_g$	0°	3.39E7 ± 0.31E7
	90°	1.18E7 ± 0.26E7

For the empty honeycomb listed in Table 3, the stiffness in the 0° direction is more than twice that in the 90° direction. When infill is added to the honeycomb and tested above T_g, a similar trend is observed. This observation suggests that the composite behaves as a mechanism in the hot state with beam bending being the dominant mode of deformation. In the cold state, however, the stiffness is nearly isotropic; indicating that beam bending is no longer the dominant mode of deformation. Below T_g the composite behaves more like a uniform mixture and Rule of Mixtures applies for calculating effective properties, yielding a modulus of 1.89E9 Pa. Failure during tensile tests typically initiated as delamination of the SMP near honeycomb joints. It was later shown through FEA and confirmed by DIC that these initiation points coincide with stress concentrations.

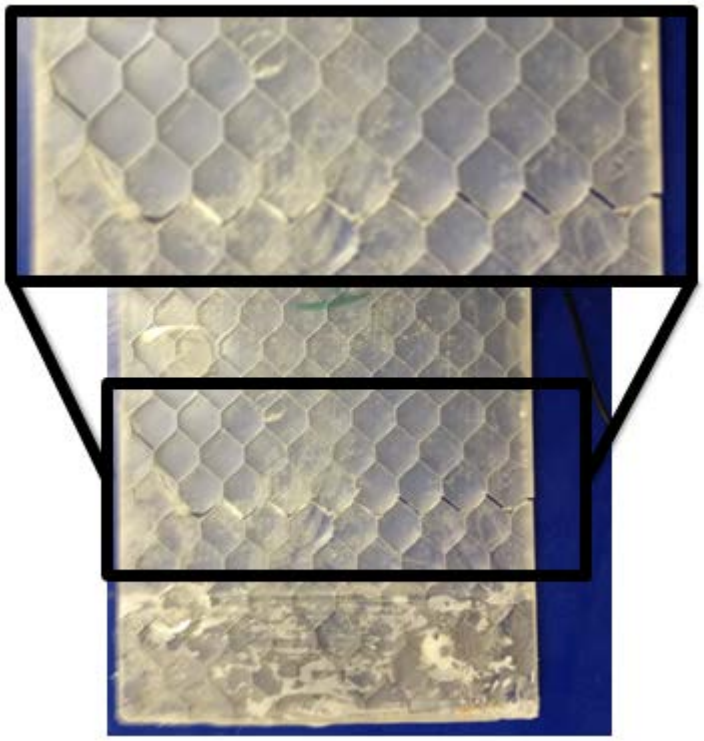

Figure 9: Typical Below T_g Tensile Failure

4.2 Composite Shear Testing

For composite shear samples, aluminum 3003 honeycomb from McMaster-Carr was cut into 12.7 cm square samples. Epoxy SMP was then poured into the Teflon mold filling the honeycomb and cured in a three step process similar to that used for tensile specimens. Finally, holes were drilled on the perimeter of the sample for attachment to the test fixture with a CNC mill and a decal applied to the front surface for tracking by the DIC system.

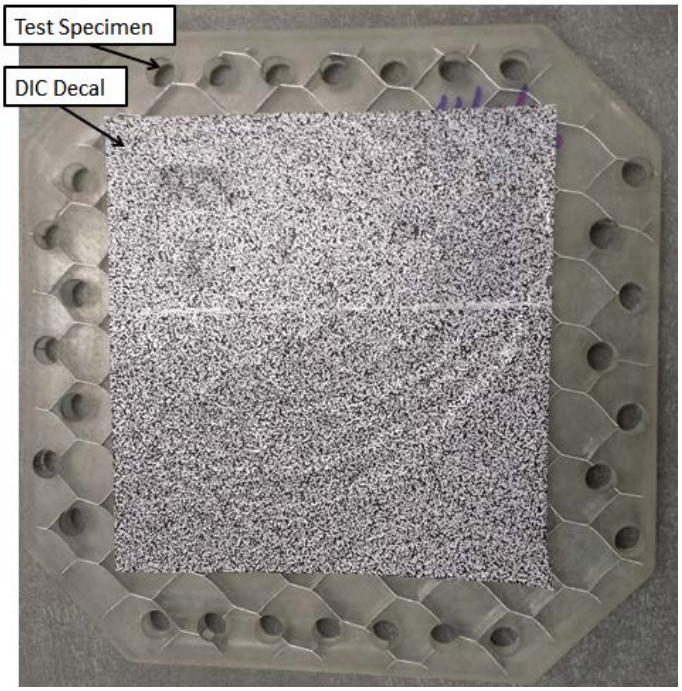

Figure 10: Shear Test Sample with DIC Decal

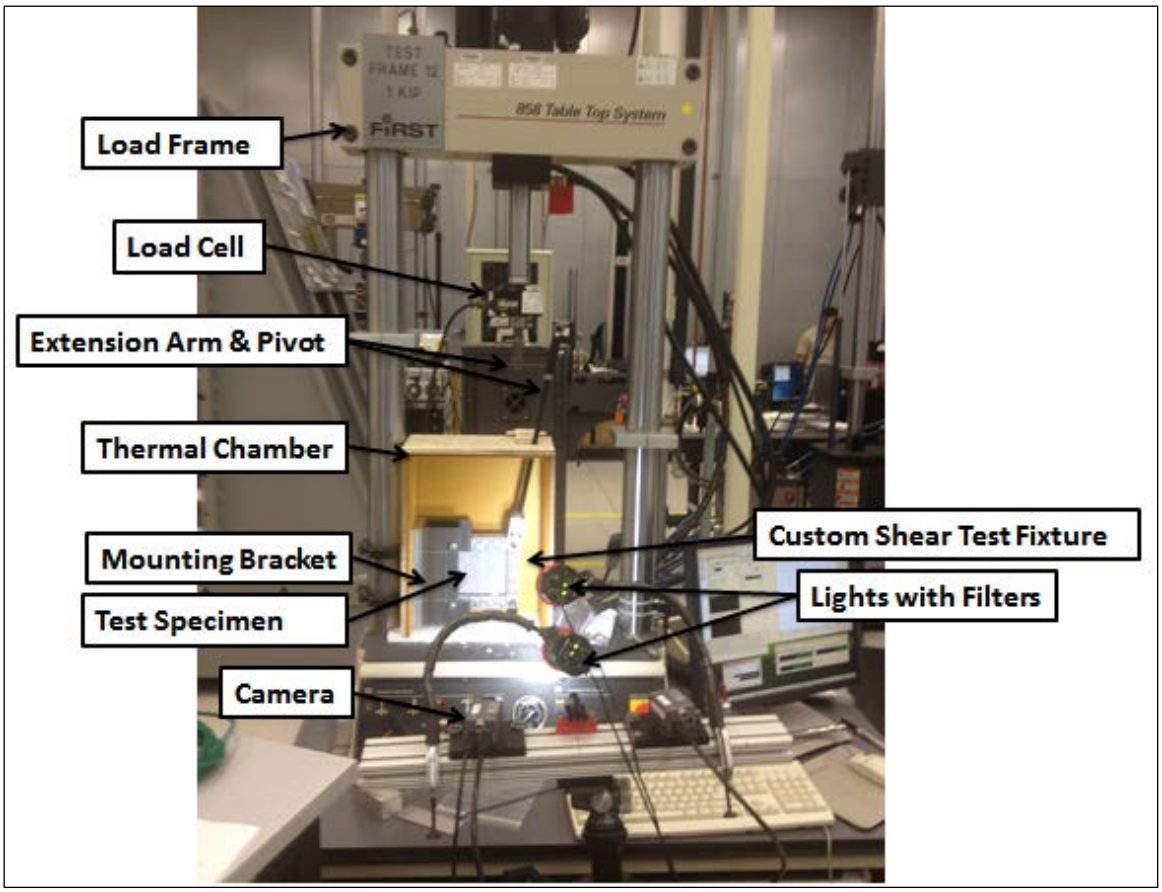

Figure 11: Shear Test SetupThe shear specimens where tested on a hydraulic MTS 858 Table Top System Model #661.19F-01 load frame with a 1000lb load cell. A custom shear test fixture was manufactured due to the anisotropic nature of the material. A detailed picture of the shear fixture is shown in Figure 12. Steel pins through the L bracket allow the four bar linkage to shear while keeping the left and right sides vertical. The extension arm displaces vertically at 12.7 mm/min and is pinned at the top to allow rotation during testing, corresponding to a shear rate of 0.1° per second. A thermal chamber was constructed of ¾ inch plywood insulated by Compression-Resistant Polyimide Insulation. The temperature was measured with k-type thermal couples and a B&K Precision 720 K-Type Thermocouple Reader. DIC was used to track strain in the sample and measure shear angle with pictures taken every four seconds, approximately 0.38°. The use of DIC allowed for an average shear angle to be measured throughout the sample and simplified the calculation of the shear modulus. Below T_g tests were conducted at ambient temperature and above T_g tests at 110°C. Finally, the shear modulus was calculated using the force measured by the load frame and the shear angle measured by DIC.

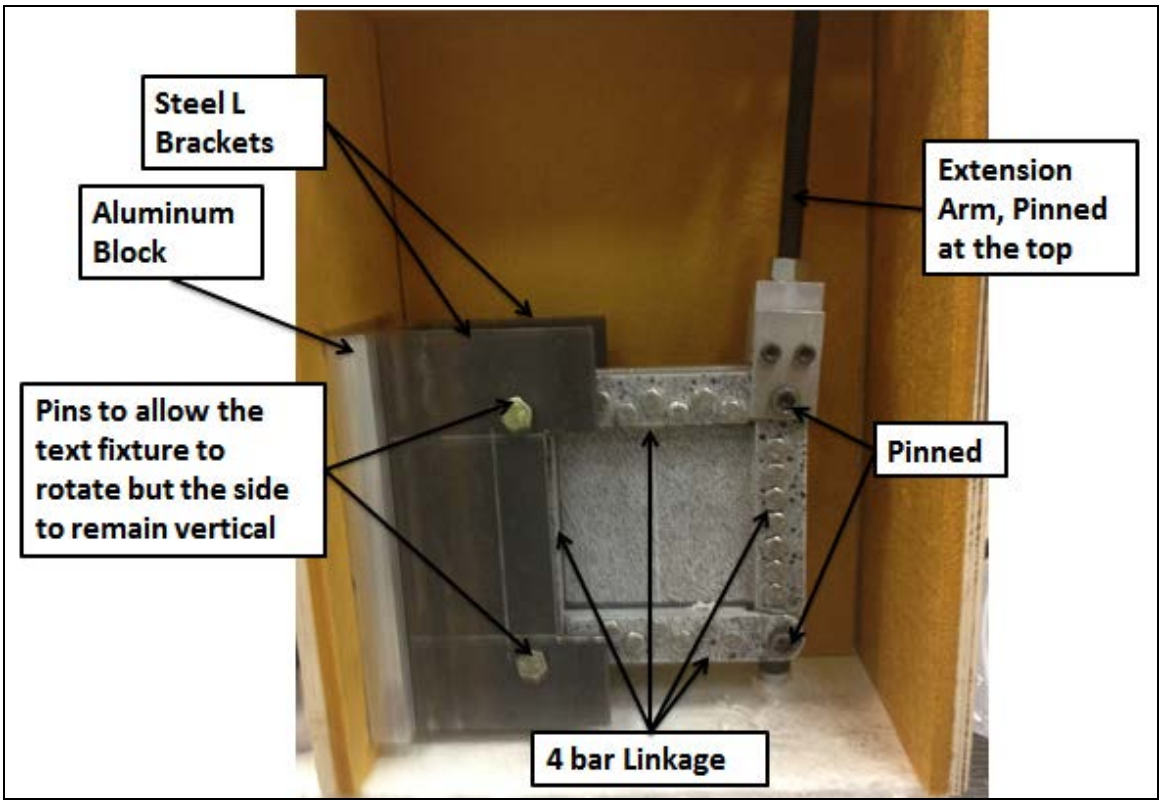

Figure 12: Shear Test Fixture

Table 5: Experimental Shear Test Results (0-90° and 90-0° directions) (Hard and Soft)

Temperature	Direction	Shear Modulus (Pa)
$< T_g$	0-90°	1.19E9±9.10E7
	90-0°	1.13E9±9.04E7
$> T_g$	0-90°	1.39E7±2.46E6
	90-0°	1.30E7±1.90E6

Table 5 are 95 percent confidence intervals. Variations in sample thickness and cell geometry are thought to be the major contributing factors in the error of the shear tests. Failure typically occurred similar to the tensile tests where delamination initiated at a stress concentration and propagated through the sample. Representative DIC shear angle results are shown in Figure 13. With the exception of the edges, the shear angle is relatively uniform over the sample ranging between 0.25° and 0.35° in any individual cell. Slight vertical columns of lower shear angle (green) can be seen, corrosponding well with those predicted by FEA in Figure 24.

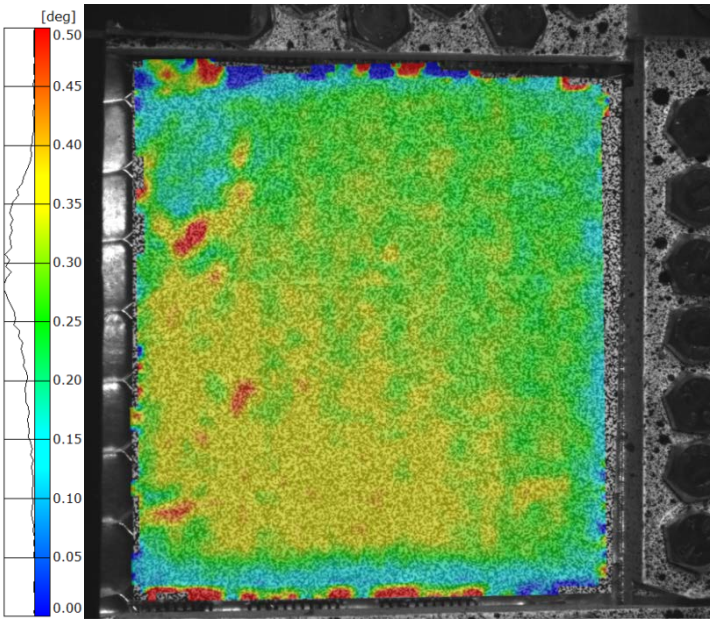

Figure 13: Typical Shear Test DIC Results (Shear Angle (deg))

4.3 Composite Experimental Conclusions

As evident from Table 4 and Table 5, the experimental honeycomb geometry used in the study is anisotropic. This is due primarily to the ratio of honeycomb side lengths, a/l, but could also be induced by angles, θ, other than 45°. The primary mode of deformation of the honeycomb when empty or filled with a low modulus material is bending. Since the bending force is proportional to the cube of length of the beam, the effective modulus of the composite Honeycomb is highly sensitive to honeycomb member lengths. Judicious choice of honeycomb geometry can thus be utilized to create an anisotropic skin when desired, leaving the skin stiff in one direction while soft in the desired direction of deformation.

Also shown in Table 5, the moduli of the composite, while anisotropic in the soft state, is nearly isotropic in the hard state, differing by less than 7 percent. This is expected since below T_g the dominant mode of deformation is no longer bending of the honeycomb members. As the stiffness of the infill approaches that of the honeycomb material, the result is an isotropic flat plate. In this scenario axial deformation dominates the response and rule of mixtures applies when calculating the effective Young's modulus. For the given experimental geometry, rule of mixtures predicts a hard state Young's modulus of 1.9E9 Pa, versus 2.2E9 Pa and 2.0E9 Pa found experimentally.

5.0 FINITE ELEMENT ANALYSIS

5.1 Overview and Assumptions

The filled honeycomb was modeled in ABAQUS v6.10 to compare to experimental and analytical results. The model was based upon homogenization theory which states a single periodic cell can be used to extrapolate the material properties if proper periodic boundary conditions are used. This reduced the size of the model and allowed the material properties to be extrapolated to a sheet of any size and not just a specific case. The unit cell geometry was based on the samples tested experimentally for direct comparison using the dimensions in Table 2. The FEA model was used to find an equivalent modulus of the skin and to investigate the mechanics of the honeycomb cell for comparison to the experimental and analytical results. Results for tensile modulus, Poisson's ratio, and shear modulus in the 0° and 90° directions above and below T_g are presented.

Implementing periodic boundary conditions in ABAQUS requires prescribing the displacement condition along the entire boundary. This negates the option of prescribing a zero stress condition on the sides of the sample as would be typical. To account for this, and to find the effective Poisson's ratio of the composite, several Poisson ratios are tested and the correct value linearly interpolated from the results until the zero stress condition on the sides of the sample is satisfied.

5.2 Composite Tensile Analysis

A strain of 0.1 percent was set for each loading case with six boundary conditions. Two boundary conditions prevented translation and rotation while the remaining four boundary conditions applied the desired loading condition. Results for Poisson's ratio and Young's moduli are listed in Table 6. Above T_g the composite behaves like a mechanism, thus the Poisson's ratios in either direction differ greatly. If the honeycomb is modeled as a series of rigid beams with pinned joints and no infill, the Poisson's ratios are calculated to be 1.71 in the 0° direction and 0.59 in the 90° direction, corroborating the notion that the composite acts like a mechanism when the infill is in the soft state.

Table 6: FEA Tensile Results

Temperature	Direction	Poisson Ratio	Young's Modulus (Pa)
$> T_g$	0°	1.61	5.0E7
	90°	0.59	
$< T_g$	0°	0.61	1.5E9
	90°	0.47	

Figure 14 shows the axial stress in the top left honeycomb beam when the composite is subjected to uniaxial tension in the 0° direction. Below T_g the stress in the beam is nearly uniform through the thickness indicating that little bending is occurring. Thus, in the hard state the composite behaves more like a typical material. Above T_g the surface of maximum stress switches between the top and bottom of the beam from one end to another, crossing and being equal near the center of the beam. Although the stress is never negative due to an offset bias, this indicates that the beam is undergoing significant bending; again supporting the notion that beam bending is the dominant mode of deformation at low infill

moduli. Under uniaxial load in the 90° direction, shown in Figure 15, the trends are very similar. The only major difference is that the location of maximum axial stress in the cold state is located near the center of the beam, as opposed to the ends as in the 0° direction load case. Above T_g, both loading cases result in high stress concentrations in the slanted members near their ends (at the joints). Although low strains were employed here, it is expected that these areas of high stress near the joints will develop into plastic hinges, save failure of another source, at higher load.

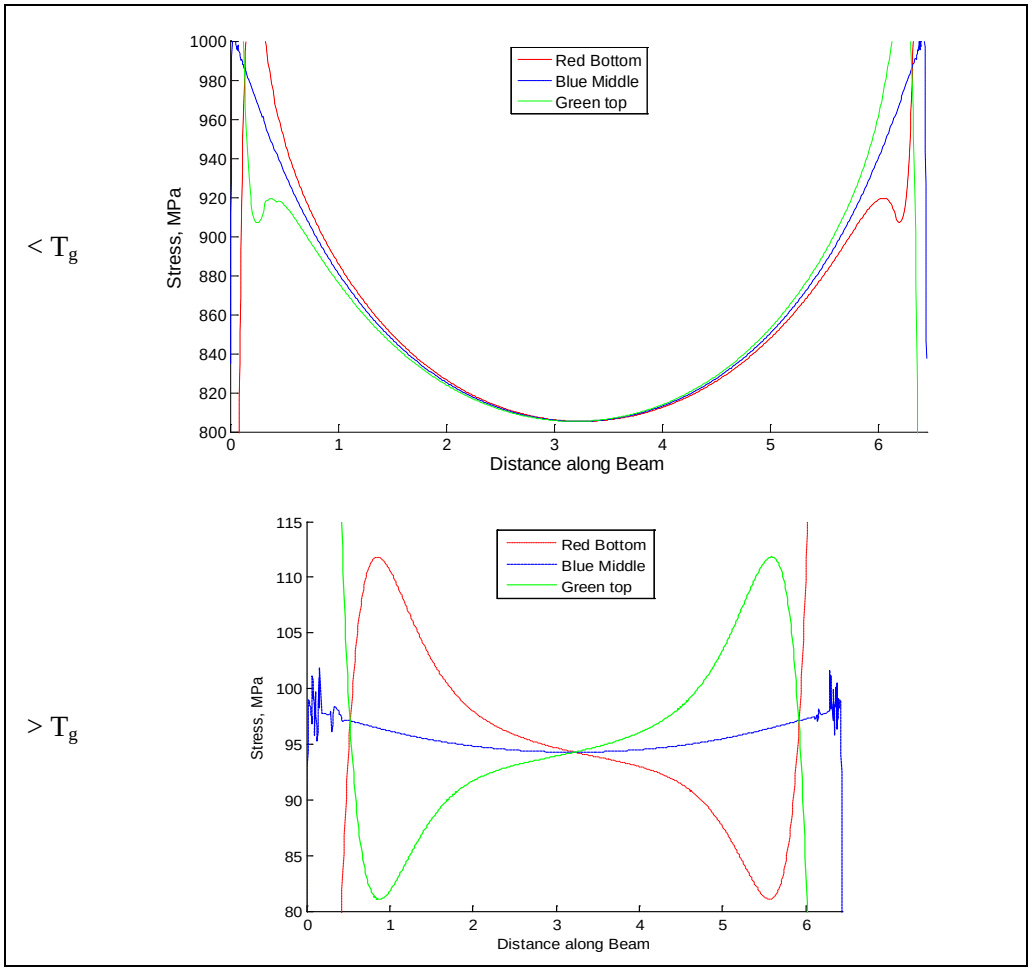

Figure 14: Axial Stress in the Top Left Slanted Honeycomb Member under Tensile 0° Load

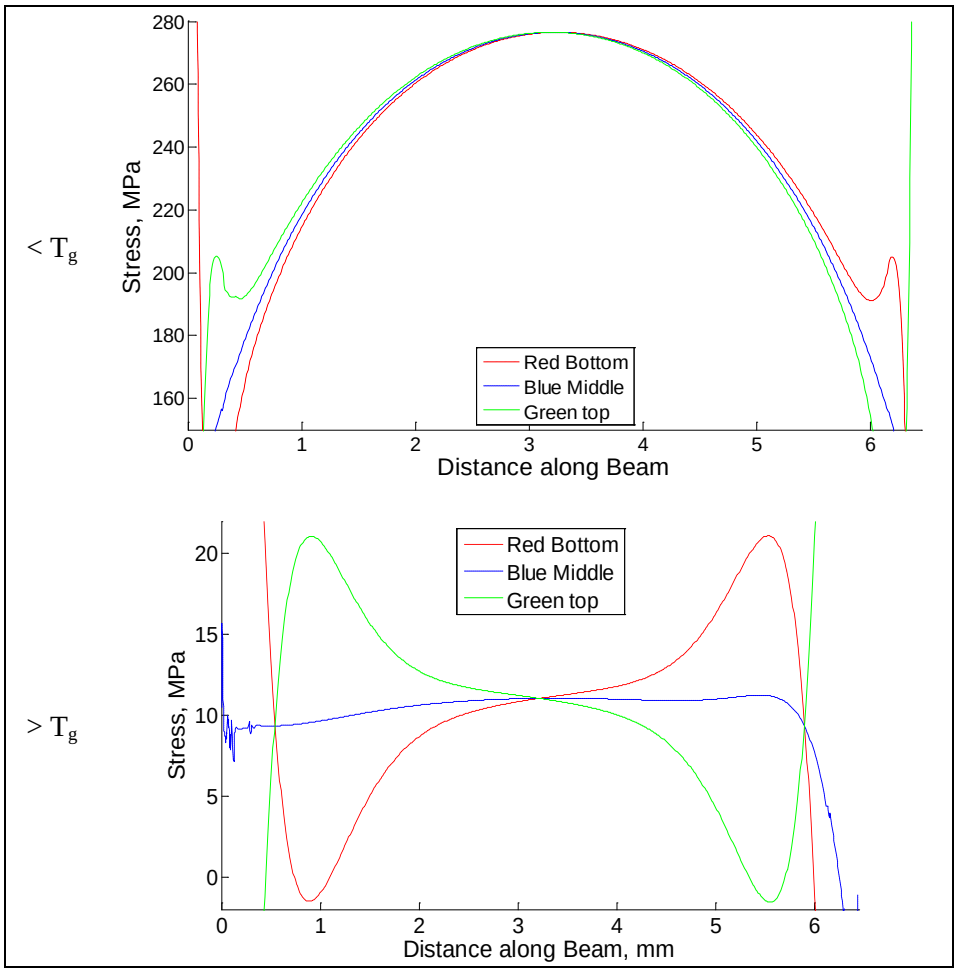

Figure 15: Axial Stress in the Top Left Slanted Honeycomb Member under Tensile 90° Load

Figure 16 and Figure 17 are the axial stress in the horizontal honeycomb members above and below T_g when loaded in the 0° and 90° directions respectively. In each case the stress is evenly distributed through the thickness of the beam indicating little to no bending. The stress in each case is also several orders of magnitude smaller than the stress found in the slanted honeycomb members of corresponding loading.

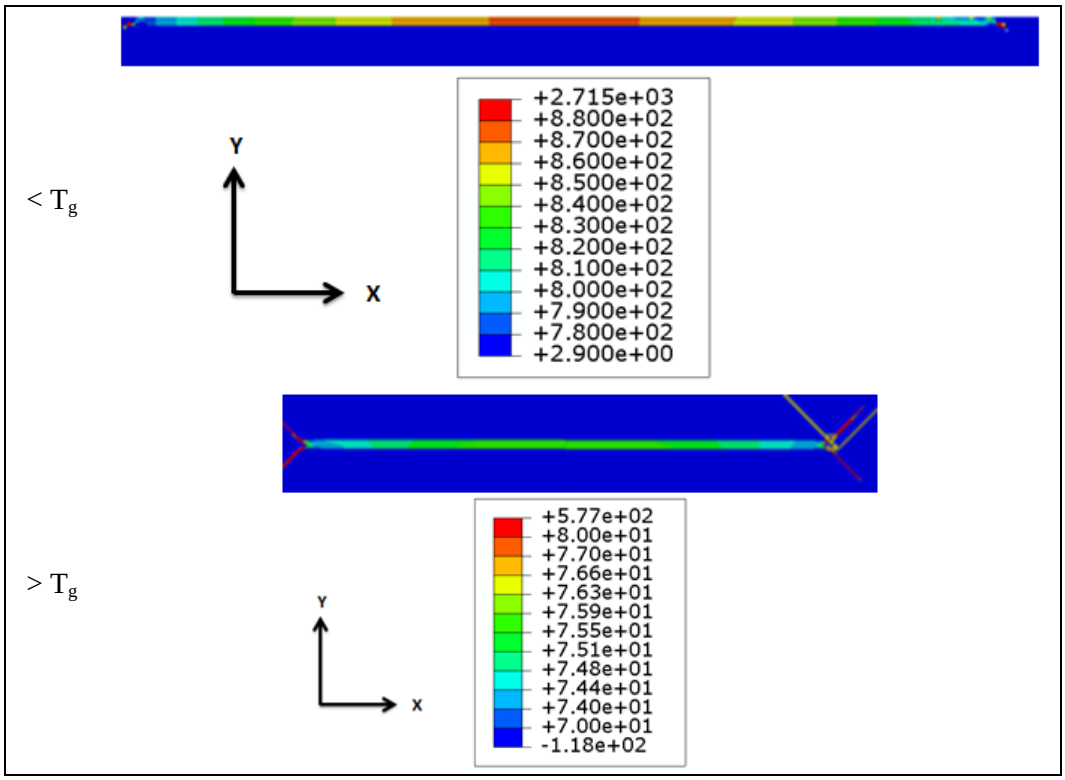

Figure 16: FEA Axial Stress in Horizontal Honeycomb Beam under 0° Tensile Load (MPa)

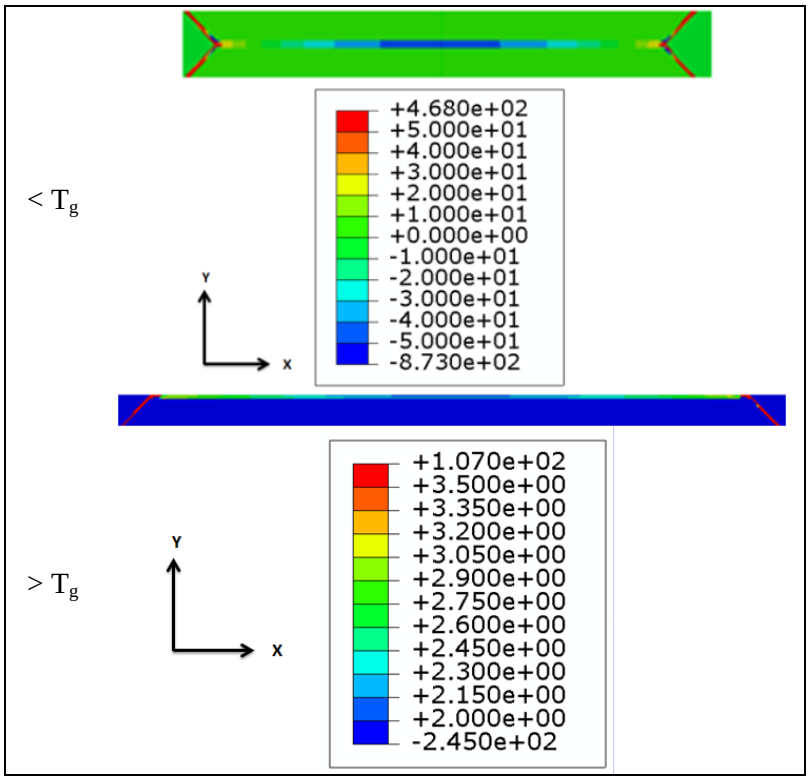

Figure 17: FEA Axial Stress in the Horizontal Honeycomb Beam under 90° Tensile Load (MPa)

Figure 18 is the Von-Mises stress distribution in the SMP under uniaxial load in the 0° direction. Both cases, above and below T_g, show stress concentrations near the honeycomb joints. The location of these stress concentrations coincides with crack initiation during experimental testing. Areas of low stress also surround the horizontal honeycomb beams in both cases, suggesting that the majority of the load is carried by the honeycomb. Under uniaxial tension in the 90° direction, Figure 19, the stresses in the infill above and below T_g is almost identical to the 0° direction loading case, both in distribution and magnitude. Below T_g this can be explained by the composite behaving similar to a standard material, where the existence of the honeycomb has a muted effect on the stress distribution. Above T_g, the composite behaves like a mechanism, so extension in the 90° direction yields similar stresses and strains as a scaled contraction in the 0° direction. Since Von-Mises stresses are necessarily positive, similar stress distributions result.

Finally, a stress concentration factor can be calculated from the FEA results. Under uniaxial tension in the 90 direction, the calculated applied stress in the soft state is 0.18 MPa. The maximum stress in the infill under these conditions was found to be 0.25 MPa, corresponding to a stress concentration factor of approximately 1.4.

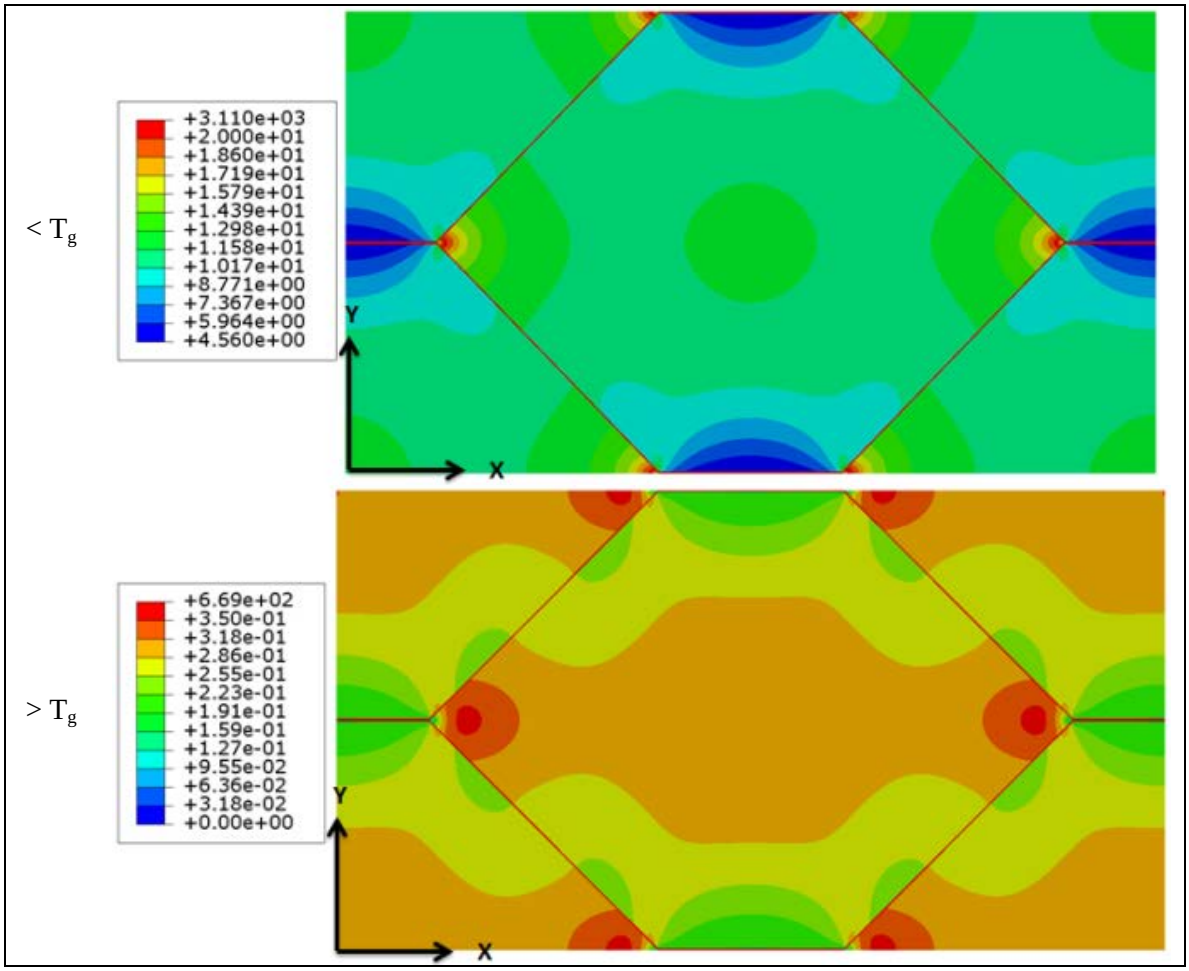

Figure 18: Von-Mises FEA Stress Prediction from Tensile Loading in the 0° Direction (MPa)

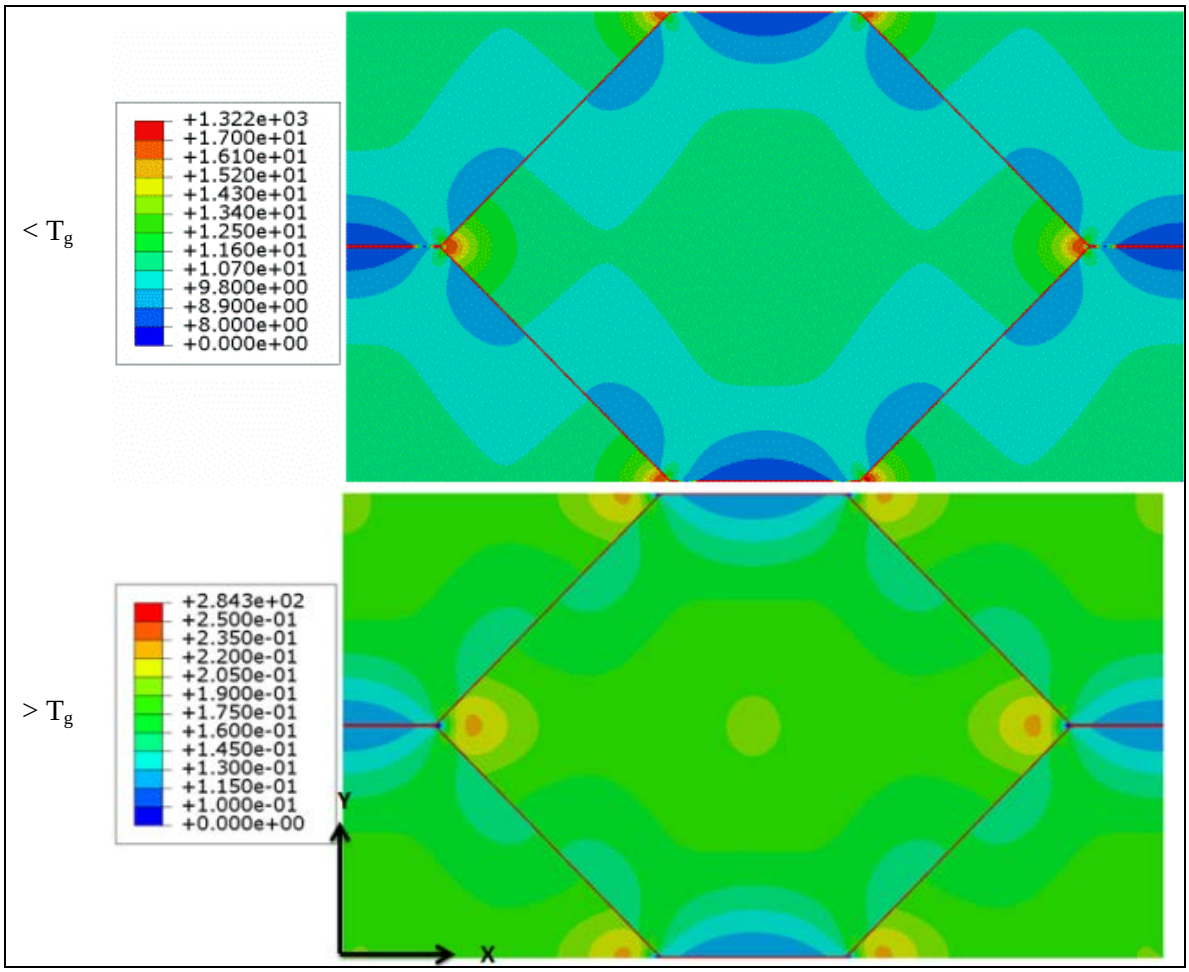

Figure 19: Von-Mises FEA Stress Prediction from Tensile Loading in the 90° Direction (MPa)

5.3 Composite Shear Analysis

Due to the material behaving like a mechanism, the response due to loading is nonlinear. Thus, a sensitivity analysis was undertaken to determine the most appropriate shear angle for calculating the shear modulus. It was shown that for the honeycomb geometry modeled, shear angles at and below 0.5° resulted in similar predictions for the modulus. The following results for the effective shear modulus of the filled honeycomb above and below T_g in 0-90° and 90-0° directions are calculated using a shear angle of 0.5°.

Table 7: FEA Predicted Shear Moduli

Temperature	Direction	Shear Modulus (Pa)
< T_g	0-90°	
	90-0°	
> T_g	0-90°	
	90-0°	

Figure 20 shows the axial stress in the top left and right slanted honeycomb members when the skin is subjected to shear in the 90-0° direction below T_g. Similar to the tensile FEA predictions, the beams

undergo little bending since at this temperature the composite behaves like a monolithic skin. While the magnitudes of stress are nearly identical, the right beam is under compression while the left beam is under tension. This is the expected result of the 90 to 0° load case.

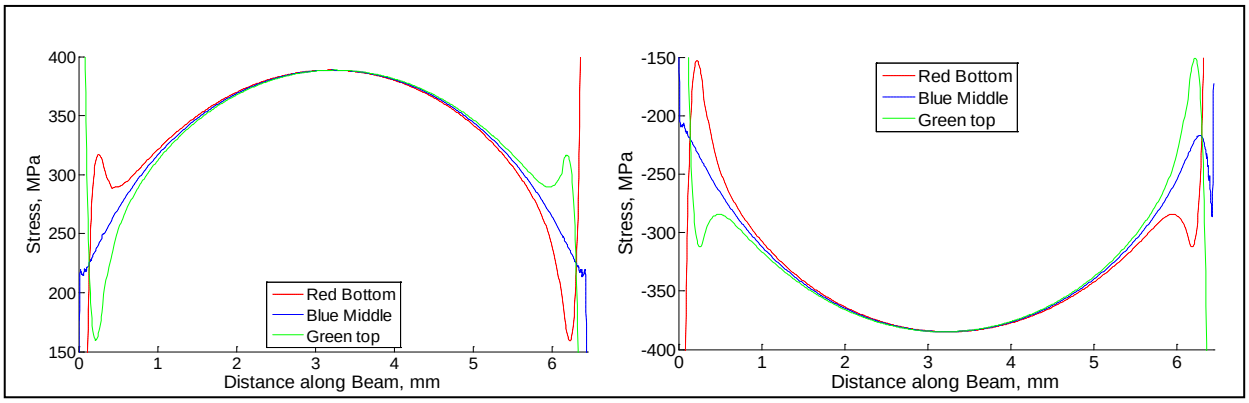

Figure 20: Axial Stress Due to 90-0° Shear Deformation <T_g
Left: Top Left Slanted Honeycomb Beam, Right: Top Right Slanted Honeycomb Beam

The horizontal honeycomb beam, however, undergoes significant bending as shown by the stress switching sign on the top and bottom surfaces, Figure 21. The large absolute stresses at either end are likely due to stress concentrations that occur at the beam joints. With the centerline at nearly zero stress, the horizontal beam is unbiased and in near perfect bending. Thus, the majority of deformation in the cold state is a result of bending of the horizontal members.

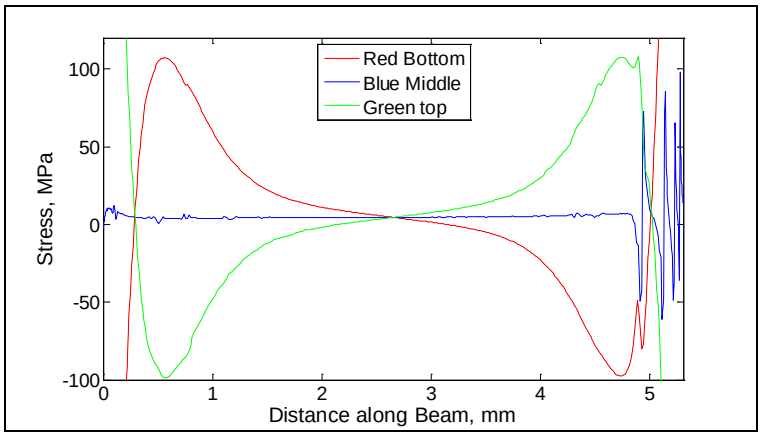

Figure 21: Axial Stress Due to 90-0° Shear Deformation <T_g in Horizontal Honeycomb BeamAbove T_g, the stress distributions in the slanted honeycomb members indicate significant bending resulting in significantly more deformation than in the cold state. The non-zero stress along the centerline of both beams signifies that they are also in net tension and compression in addition to bending. It should be noted that the top left slanted honeycomb member is identical to the bottom right slanted honeycomb member (not shown), as are the top right and bottom left members. Every horizontal member is also identical. As with the tensile tests, it is believed that the high stresses at the joints will result in plastic joints with increased deformation.

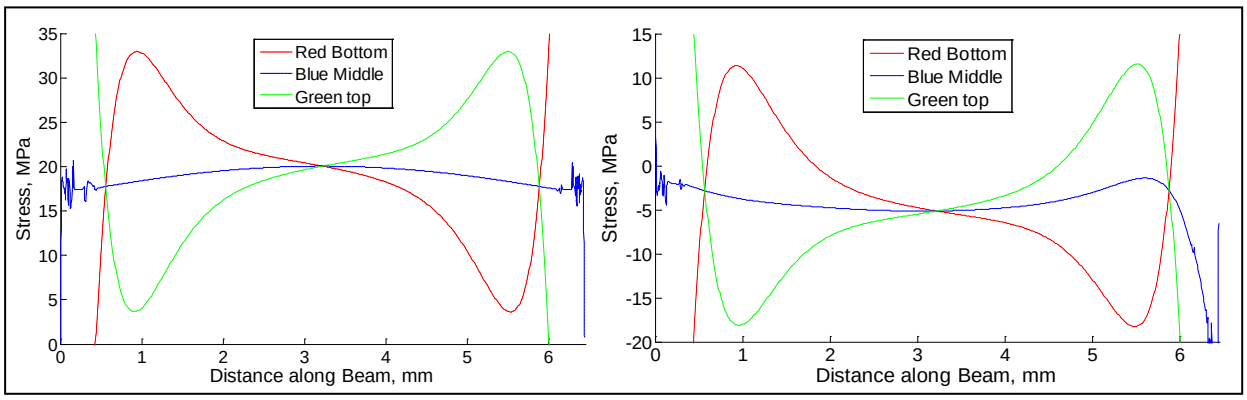

Figure 22: Axial Stress Due to 90-0° Shear Deformation >T_g
Left: Top Left Honeycomb Beam, Right: Top Right Honeycomb Beam

Below T_g, the minimum and maximum shear stress in the infill differ by approximately an order of magnitude. In Figure 23, notice the vertical columns of shear stress, also seen experimentally in Figure 13. In is interesting to note that the shear stress in the infill both above below T_g near the slanted honeycomb members is nearly zero, while the shear stress in the infill near the horizontal members is non-zero. This is a result of the major mode of deformation of the composite being a result of bending of the horizontal members. Thus in tension, the slanted honeycomb members are responsible for deformation while in shear the horizontal members are responsible for deformation.

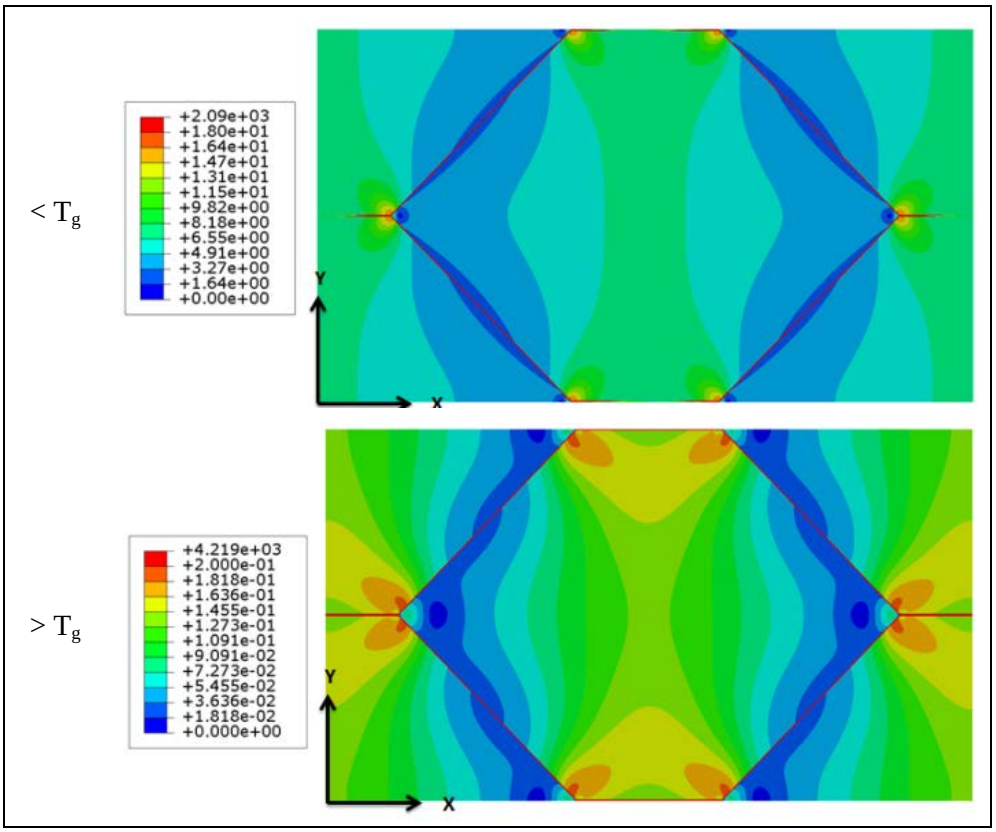

Figure 23: FEA Von-Mises Stress Prediction under 90-0° Shear Load (MPa)

Figure 24 shows the shear stress induced in the composite due to an applied shear strain. Comparing Figure 24 with Figure 23 it is clear that the shear stress in the composite is the dominating stress, as the two distributions are nearly the same, although the magnitude of the shear stress is slightly lower.

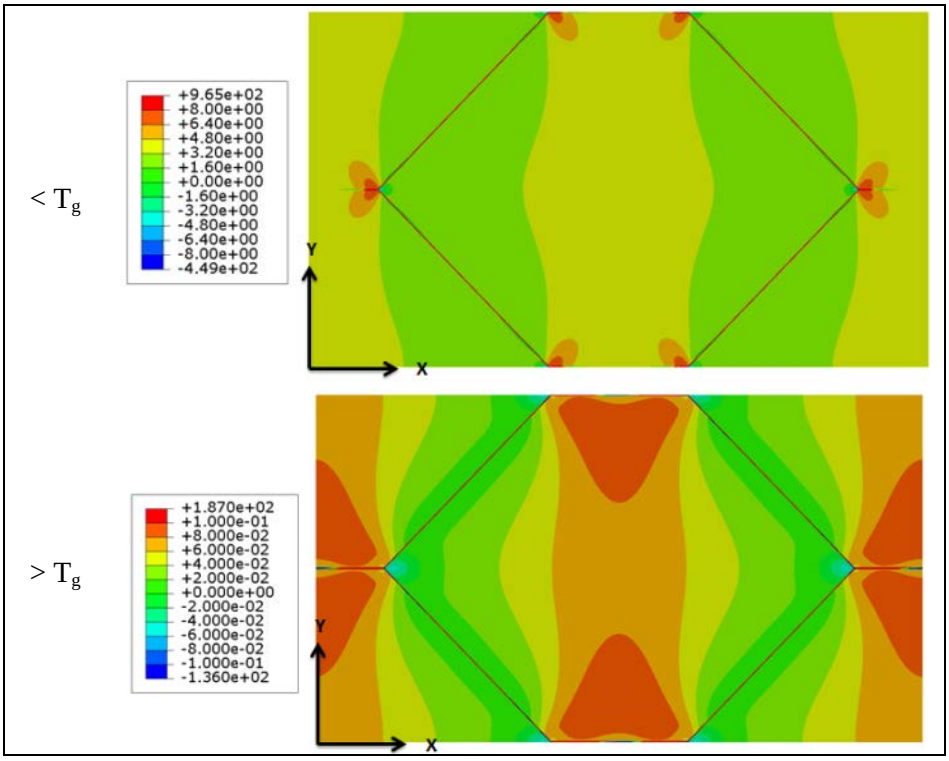

Figure 24: FEA 90-0° Shear Stress Prediction under 90-0° Shear Load (MPa)

6.0 MODELING AND OPTIMIZATION

6.1 Filled Honeycomb Model

El-Sayed et al developed equations for a honeycomb with a low modulus infill. (El-Sayed, 1979) He assumed that the deformations remained small and the sides of the hexagon remained straight due to the infill. Other implied assumptions included thin beam theory, that the honeycomb was perfectly elastic, the honeycomb is completely uniform, and perfect adhesion between the infill and honeycomb. He then used Castigliano's method to calculate the deformation of the honeycomb.

$$q_i = \frac{\partial U}{\partial F_i}, i = 1,2, \ldots p \tag{2}$$

Where U is strain energy and q is the deformation at the applied load, F. For simplicity, axial deformation of the honeycomb walls is neglected. Figure 5 shows the unit cell and variable definitions used in the model. x_o and y_o are a function of the cell geometry used to simplify the equations. The energy in the infill is then calculated by integrating over the volume assuming the sides remain straight. Forcing the deformation of the honeycomb to equal that of the infill, the total strain energy is then found and the effective modulus of the filled honeycomb calculated as:

$$E_{x_c} = B_H E_H + B_I E_I \tag{3}$$

$$E_{y_c} = D_H E_H + D_I E_I \tag{4}$$

Where E is Young's modulus and the subscripts H and I represent honeycomb and infill quantities. B_H, B_I, D_H, and D_I are geometric weighting factors and are calculated as:

$$B_H = \frac{(a + x_0)}{y_0\left(\frac{y_0^2 l}{d^3} + \frac{x_0^2}{ld} + \frac{a}{d}\right)} \tag{5}$$

$$B_I = \frac{(a + x_0)K}{2(1 - \nu_i^2)\frac{y_0^3}{x_0^2}} \tag{6}$$

$$D_H = \frac{y_0}{(a + x_0)\left(\frac{x_0^2 l}{d^3} + \frac{y_0^2}{ld}\right)} \tag{7}$$

$$D_I = \frac{y_o[K]}{2(a + x_o)(1 - v_i{}^2)} \tag{8}$$

K is defined as:

$$[K] = \left[\left(\frac{y_o}{x_o}\right)^3 - \frac{a}{x_o}\left(\frac{y_o}{x_o}\right)^3 + \frac{1}{2}\left(\frac{a}{x_o}\right)^2\left(\frac{y_o}{x_o}\right)^3 \ln\left(1+\frac{2x_o}{a}\right) + \frac{x_o}{y_o} + \frac{a}{y_o} + 2\upsilon_i\frac{y_o}{x_o} \right] \quad (9)$$

Where I is the second moment of area about the minor axis of the beam, A is the cross-sectional area of the beam, E_H and E_I are the elastic moduli of the honeycomb and infill respectively, and υ_i is Poisson's ratio of the infill. This model is limited to deformations of about 30 percent strain and for composites where the infill is at least four orders of magnitude below that of the honeycomb. El-Sayed experimentally verified his model using an aluminum honeycomb and Flexane30 infill; whose geometry and properties are listed in Table 8 with the results of effective modulus versus applied strain shown in Figure 25: . Although a standard honeycomb geometry was used, which masks anisotropic behavior, the model matches well with the experimental results in the elastic and plastic strain regions.

Table 8: El-Sayed Experimental Parameters

a Horizontal Wall Length (mm)	l Slanted Wall Length (mm)	d Wall Thickness (mm)	θ Interior Angle (deg)	E_H Honeycomb Young's Modulus (GPa)	E_I Infill Young's Modulus (MPa)
7.3	7.3	0.1	60	70.3	1.08

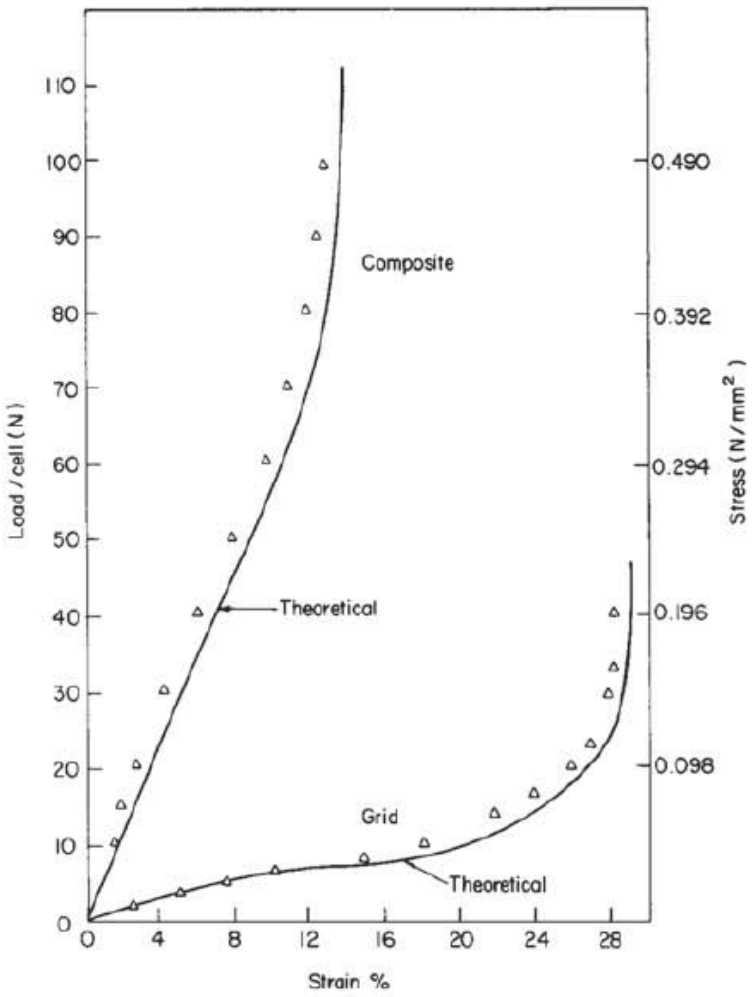

Figure 25: Experimental Results of Flexane30/Aluminum Honeycomb Composite (El-Sayed, 1979)

El-Sayed's model predictions using Equations (3) and (4), the geometry listed in Table 2, infill moduli listed in Table 1, and an aluminum 3003 modulus of 73.1 GPa are listed in Table 9.

Table 9: El-Sayed Model Predictions

Temperature	Direction	Tensile Modulus
$< T_g$	0°	4.9 GPa
	90°	1.7 GPa
$> T_g$	0°	71.5 MPa
	90°	24.9 MPa

6.2 Plate Deflection Model

The design application for the proposed honeycomb system is the skin of a reconfigurable aircraft wing adhering to the MAS Phase II program parameters stating that the skin is rigidly supported by a 15- by 20-inch frame and must support an aerodynamic load of 400 lb/ft^2 with a maximum deflection less than 0.1 inches. (Asheghian, Reich, Enke, & Kudva, 2011) To calculate the deflection of the panel, Puttmann

et al derived an equation for an anisotropic plate using Castigliano's method: (Puttmann, Beblo, Joo, Smyers, & Reich, 2012)

$$\delta = \frac{2m^2b^2}{5c^3(m+b)^3}\left[\frac{M_{bcv}(3m+b)}{E_{cy}} + \frac{M_{mcv}(m+3b)}{E_{cx}}\right] \tag{10}$$

Where m is the long side of the panel, b is the short side of the panel, c is the depth of the panel, M_{bcv} and M_{mcv} are internal moments, E_{cy} and E_{cx} are the Young's moduli of the panel in each in-plane direction, and δ is the center point deflection of the panel. The bending moments in the plate are related to the uniform pressure load through:

$$M_{bcv} = 0.009wb^2(1+2\alpha^2-\alpha^4) + \frac{v_i wb^2}{8(3+4\alpha^4)} \tag{11}$$

$$M_{acv} = \frac{wb^2}{8(3+4\alpha^4)} + 0.009v_i wb^2(1+2\alpha^2-\alpha^4) \tag{12}$$

where w is the pressure applied to the panel, v_i is Poisson's ratio of the equivalent honeycomb composite, and α is the ratio:

$$\alpha = \frac{b}{m} \tag{13}$$

If E_{xc} and E_{yc} are equal, the maximum deflection of the plate calculated by equation (10) differs from that by flat plate theory of an isotropic material by less than 2%. Using Equations (10) through (12) for the deflection of the panel, the panel dimension prescribed by the MAS program of 0.508 by 0.381 m, the honeycomb geometry listed in Table 2, and effective in-plane moduli calculated by El-Sayed listed in Table 9; the skin would have to be 43.8 mm (1.72 in) thick to satisfy a panel center point deflection of less than 2.54 mm (0.1 in) under a 400 lb/ft^2 pressure load if every cell was above T_g. At such a thickness, the skin would far exceed the weight requirement. To reduce the thickness and thus the weight, future studies will investigate the advantages of heating only certain cells in particular patterns, thus increasing the bending stiffness of the skin while retaining low in-plane stiffness in the desired direction.

6.3 Filled Honeycomb Optimization

To increase flexibility of the system and decrease weight, it is possible to take advantage of the highly anisotropic nature of honeycomb when customizing the geometry for a specific application. For the presented example case of the skin of a reconfigurable wing, the honeycomb unit cell geometry was optimized to minimize the sum of the effective Young's moduli in the x and y directions. This ultimately reduces the actuation energy needed to reconfigure the composite skin.

6.3.1 Boundary Conditions and Objective

The design variables are the horizontal wall length, a, slanted wall length, l, wall thickness d, and cell angle, θ. The depth of the cell was not included because it is directly related to the applied aerodynamic load and in plane effective moduli. Consequently the weight of the skin is not directly calculated here. The objective function shown in Equation (14) was chosen as a simplified representative option. The

design for a particular application will involve many different wing shapes, resulting in many different optimization functions that the designer must weight against each other.

$$E_{c_x} + E_{c_y} \tag{14}$$

The cell angle was constrained to below 75° due to limitations discovered with El-Sayed's model, Equations (3) and (4) and above 55° to maintain the desired strain capability. The cell wall thickness, *d*, had a lower bound constraint of 0.2 mm, which is the lowest manufactured honeycomb cell wall width available. The the horizontal and slanted wall lengths were constrained to be less than 100 mm to maintain a desired maximum cell size.

The optimization was run with MatLAB© Optimtool which accepts upper and lower bounds for the design variables and nonlinear equalities. Optimtool selects the 'best' algorithm to use which was a mixture of the sequential quadratic programming, Quasi-Newton, and line search algorithms.

6.3.2 Optimized Geometry

The optimization showed that the most influential quantities on the effective composite moduli were the wall thickness and the internal angle θ with the largest contributing factor being the wall thickness. This is expected since the major mode of deformation of the honeycomb with a soft infill is bending and the force due to bending scales with wall thickness cubed. Various initial starting point geometries were used resulting in different optimized solutions with θ consistently limited by its upper bound constraint. Interestingly, the ratio of *a:l* and *a:d* were constant for each solution at 0.3 and 26.4. Presented in Table 10, are two sets of results that have a ratio of 0.3 and 26.4 respectively. Note that the moduli are the same.

Table 10: Optimal Honeycomb Geometry

E_{xc} (GPa)	E_{yc} (GPa)	θ (deg)	l (mm)	d (mm)	a (mm)
1.55	1.36	75	16.19	2.01	52.8
1.55	1.36	75	1.619	0.201	5.28

7.0 DISCUSSION/CONCLUSIONS

7.1 Modeling Limitations

While the above method has proven useful for determining trends, there are several limitations and inherent errors associated with each element. Experimentally, there was a moderate amount of inconsistency observed in the honeycomb cells, increasing the confidence level of the results. Although the ASTM standard was adhered to, there is also uncertainty in the edge effects of the honeycomb, or partial cells lining the edge of each sample. Due to availability and the significant effort required, only one honeycomb geometry was experimentally characterized. A single data point is clearly insufficient to validate an analytical model meant to predict the effective moduli of the skin for a large range of honeycomb geometries. Higher quality manufacturing is expected to have a large impact on the strength of the honeycomb and composite.

The analytic model is possibly the weakest link in the analysis. It doesn't take into account the strength between layers of the honeycomb or adhesion strength between the SMP and the honeycomb. It also cannot take into account the possibility of a non-uniform temperature distribution within each cell; which would result in non-uniform material properties of the infill. The model also greatly overestimates the stiffness of the composite predicting nearly double the experimental and FEA results, Table 11. The model as published also does not predict shear stiffness of the composite which, for reconfigurable aircraft wings, is possibly more important than tensile strength. Finally, because the model is based on the principle that bending of the honeycomb beams is the dominant mode of deformation, it is incapable of modeling the composite as the infill modulus approaches that of the honeycomb. As the infill becomes stiffer, the composite approximates an isotropic flat plate and the mechanism of deformation changes. This would be true for nearly any analytic model, however. An analytic model is required for optimization and thus the limitations are acceptable given the predicted trends are correct.

Table 11: Young's Modulus (Pa)

Temperature	Direction	Experimental	Analytic Model	FEA Model
< Tg	0°	2.19E9	4.9E9	1.5E9
	90°	2.04E9	1.7E9	
> Tg	0°	3.39E7	7.15E7	5.0E7
	90°	1.18E7	2.49E7	

Table 12: Shear Modulus (Pa)

Temperature	Direction	Experimental	Analytic Model	FEA Model
< Tg	0-90°	1.19E9	NA	
	90-0°	1.13E9	NA	
> Tg	0-90°	1.39E7	NA	
	90-0°	1.30E7	NA	

The FEA model is also limited by the assumptions of perfect adhesion, manufacturing, non-uniform geometry, and non-uniform thermal/material property distribution. The FEA model is not required for optimization; however it is useful for validating the analytic model for geometries that cannot feasibly be

tested experimentally. There also inherent errors with modeling a 3D system in 2D. The predicted stress may be higher than seen experimentally because the infill material is restricted from out-of-plane deformation.

The optimization both inherits the errors and limitations of the analytical model as well as introduces new errors and limitations. It doesn't account for non-uniform honeycomb geometry, non-uniform temperature distributions within the cells, and does not allow for non-uniform heating of the skin using the cells to create a pattern of soft and hard material. The optimization also becomes exponentially more complicated if more than one wing shape is considered simultaneously.

7.2 System Results and Future Work

In general the modeling and optimization scheme is relatively accurate, correctly predicting the trends of the system. While the absolute values in some cases do not match and may not precisely reflect a real system; the result is optimized and the best possible design given the constraints. The model has shown that it is possible to judiciously design a system to take advantage of the anisotropic nature of honeycomb for specific applications. The extremely high effective Poisson's ratio, 1.61, that arises from the composite behaving like a mechanism can in some cases be a limiting factor while in others be used to the designer's advantage. Different materials, such as phase changing materials like waxes, could also be used to further expand the application of the skin. Although the current model assumes the infill completely fills the honeycomb; to reduce weight the infill could be limited to the surface of the honeycomb leaving the center void, effectively resulting in a sandwich structure.

While the presented research represents a comprehensive initial feasibility study into the proposed filled honeycomb skin system, there are many topics that need developed more thoroughly. The current work does not investigate thermal issues in any detail. How to quickly and evenly heat the SMP within each cell, thermal diffusion between cells, cooling the skin, the power required for operation, and cycle time are topics of further research. The study also does not include the possibility that each cell of the skin may be made a different temperature and thus have different mechanical properties. Heating patterns may lead to more efficient systems allowing for reduced power loads and system weight. It may also allow the skin to operate in unique loading conditions. A more accurate and flexible analytic model would also allow a broader range of conditions to be studied and result in more accurate system capabilities. All of these topics will need to be addressed in detail before the system is operational and ready to be deployed in the field.

REFERENCES

Abd El-Sayed, F., Jones, R., & Burgess, I. (1979, October). A Theoretical Approach to the Deformation of Honeycomb Based Composite Materials. *Composites*, 209-214.

Andersen, G., & Cowan, D. (2007). Aeroelastic Modeling Analysis and Testing of a Morphing Wing Structure. *AIAA/ASME/ASCE/AHS/ASC Structres, Structural Dynamics, and Materials Conference.* Honolulu, Hawaii: AIAA.

Asheghian, L., Reich, G., Enke, A., & Kudva, J. (2011, June). Shear Morphing Skins - Simulation and Testing of Optimized Design. *Journal of Intelligent Material Systems and Structures, 22*, 945-960.

Puttmann, J., Beblo, R., Joo, J., Smyers, B., & Reich, G. (2012). Design of a Morphing Skin by Optimizing a Honeycomb Structure with a Two-Phase Material Infill. *Smart Materials, Adaptive Structures, and Intelligent Systems.* Stone Moungtain, GA.

Xie, T., & Rousseau, I. A. (2009). Facile Tailoring of Thermal Transition Temperatures of Epoxy Shape Memory Polymers. *Polymer*, 1852-1856.

LIST OF ACRONYMS, ABBREVIATIONS, AND SYMBOLS

ASTM	American Society for Testing and Materials
CNC	Computer Numerical Control
DIC	Digital Image Correlation
FEA	Finite Element Analysis
GM	General Motors
MAS	Morphing Aircraft Structures
SMP	Shape Memory Polymer

VARIABLES/SYMBOLS

A	Cross-Sectional Area
B	Geometric Coefficient
D	Geometric Coefficient
E	Young's Modulus
F	Point Load
I	Second Moment of Area
K	Geometric Coefficient
M	Internal Moment
S	Fitting Variable
T	Temperature
T_g	Polymer Transition Temperature
U	Strain Energy
θ	Honeycomb Interior Angle
a	Horizontal Honeycomb Member Length
b	Short Side of Panel Length
c	Honeycomb Depth
d	Honeycomb Member Thickness
l	Slanted Honeycomb Member Length
m	Long Side of Panel Length
q	Point Deflection
w	Aerodynamic Pressure Load
α	b/m
δ	Deflection
ν	Poisson's Ratio

SUBSCRIPTS

C	Cold State/Composite Quantity
H	Hot State/Honeycomb Quantity
I	Infill Quantity
x	0° Direction
y	90° Direction